**Title page**

# Reinforced anticorrosion performance of waterborne epoxy coating with eco-friendly L-Cysteine modified $Ti_3C_2T_x$ MXene nanosheets

Sihao Li [a, ‡], Haowei Huang [b, c, ‡], Xiaoling He [a], Yanqi Ma, Ying Chen [a], Li Zhang [a], Xinxin Sheng [a, *], Elena Shchukina [c], Dmitry Shchukin [c]

[a] *Guangdong Provincial Key Laboratory of Functional Soft Condensed Matter, School of Materials and Energy, Guangdong University of Technology, Guangzhou, 510006, China*

[b] *School of Chemistry and Chemical Engineering, Guangdong Provincial Key Lab of Green Chemical Product Technology, South China University of Technology, Guangzhou, 510640, China*

[c] *Stephenson Institute for Renewable Energy, Department of Chemistry, University of Liverpool, Crown Street, Liverpool L69 7ZD, UK*

[d] *Yunnan Provincial Key Laboratory of Energy Saving in Phosphorus Chemical Engineering and New Phosphorus Materials, The Higher Educational Key Laboratory for Phosphorus Chemical Engineering of Yunnan Province, Kunming 650500, China*

‡ Sihao Li and Haowei Huang contributed equally to this work.

* Corresponding author. E-mail: xinxin.sheng@gdut.edu.cn (X.S.)

**Abstract**

In this study, MXene ($Ti_3C_2T_x$) nanosheets were modified by an amino acid (L-Cysteine) to fabricate functionalized MXene (fMX) hybrid material. Results derived from FTIR, XRD, EDS and XPS confirm that L-Cysteine has succeeded in covalently functionalizing MXene's surface. Later, fMX was introduced into the waterborne epoxy (WEP) coating as fillers, and its anti-corrosion performance was studied through electrochemical impedance spectroscopy and potentiodynamic polarization tests. After being immersed in 3.5 wt.% NaCl solution for 30 days, fMX/WEP still maintains a higher impedance modulus at lowest frequency ($1.21\times10^9\ \Omega\cdot cm^2$) and a lower corrosion rate ($7.95\times10^{-6}$ mpy) compared to blank WEP. It is resulted from the well dispersion of fMX nanosheets in WEP matrix as well as the enhanced barrier properties offered by fMX. Our research provides a promising strategy for green modified MXene to improve the corrosion resistance of the coating.

**Key words:** $Ti_3C_2T_x$ MXene, Functionalization, Waterborne epoxy coating, Corrosion resistant, L-Cysteine

## 1. Introduction

Corrosion has caused serious safety hazards, environmental pollution and huge economic losses for many decades. It is estimated that the annual economic losses caused by corrosion even exceed 3% of global GDP [1–3]. Applying organic coating on the surface of metal substrate is a cost-effective and widely-used anti-corrosion method [4–6]. Organic epoxy coatings are widely used owning to their excellent performance, such as good adhesion on the substrate, high crosslinking density, excellent chemical and weather resistance [7–9]. But traditional solvent borne coatings normally contain high volatile organic compounds (VOCs), out of the increased awareness of environmental protection, environmentally friendly waterborne epoxy coatings (WEP) have attracted attention [10,11]. However, micropores and microcracks are generated in the WEP coating because of the evaporation of the water during the curing process through which corrosive media (e.g., $H_2O$, $O_2$ molecules, $Cl^-$ ions, etc.) easily penetrates into metal surface and trigger corrosion [12,13].

Introducing two-dimensional (2D) nanomaterials into WEP coatings is a most promising way to improve its corrosion resistance [14,15]. 2D nanomaterials with high specific surface area, such as graphene, graphene oxide (GO), hexagonal boron nitride (h-BN) and 2D transition metal carbides (MXenes), were added into organic coatings to increasing the path of corrosive electrolyte in the coating. However, the dispersibility and compatibility of 2D materials in organic polymer matrix affect its barrier performance [16–18]. Surface modification of 2D materials is a potential solution of this problem. Ramezanzadeh et al. [19] functionalized GO with *p*-phenylenediamine

(PPDA) and, as a result of that, the barrier and corrosion protection performance of the coating with PPDA-GO was improved. Pourhashem et al. [20] selected (3-aminopropyl) triethoxysilane (APTES) for modifying GO flakes (A-GO). The results showed that not only the compatibility and interfacial interaction of A-GO in polymer coating were improved but also corrosion resistance and adhesion strength to metal substrates of A-GO/epoxy composites were strengthened.

As a mixture of 2D transition metal carbides, nitrides and carbonitrides, MXenes is a new 2D material first discovered by Gogosti in 2011 [21]. Its general formula is $M_{n+1}X_nT_x$, where M stands for the early transition metal (Sc, Ti, Zr, etc.), X is C, N or CN, n=1, 2 or 3 and T means the surface termination groups (such as hydroxyl, oxygen or fluorine) [22]. MXene has high surface area, excellent hydrophilicity and abundant surfaces functionality [23–25]. Yan et al. [26] incorporated $Ti_3C_2$ nanosheets as physical barrier to epoxy coatings, which exhibited significantly higher corrosion resistance than blank epoxy coatings. Yan et al. [27] reported that the composite coatings containing amino-functionalized MXene has perfect anti-corrosion and tribological properties because of the good dispersity of fillers in polymer matrix and the high adhesion strength between coating and metal substrate. Although the significance of amino-functionalization on MXene is obvious, the widely used amine compound modifiers are usually synthetic and unsustainable [28,29]. There is an urgent need to find a bioreagent that is environmentally friendly, easy to access and good for corrosion protection.

L-Cysteine, an amino acid with one sulfhydryl group at the end, is widely used as a green corrosion inhibitor [30–33]. Wang et al. [34] studied the inhibition effect and

reaction mechanism of L-Cysteine on the corrosion of bronze covered with a CuCl patina. They found that L-Cysteine effectively inhibited the hydrolysis reaction of CuCl at up to 90% efficiency. Stimpfling et al. [35] intercalate L-Cysteine into a layered double hydroxide (LDH), and then dispersed it into epoxy based primer layer as an ion exchange inorganic functionalized filler. L-Cysteine was released from the LDH containers during the corrosion process to delay or even terminate corrosion reaction. Here, we use L-Cysteine as surface modifier of MXene to improve the dispersion performance of MXene in the epoxy matrix, thereby improving the anti-corrosion performance of waterborne epoxy coatings.

In the present paper, few-layered MXene ($Ti_3C_2T_x$) nanosheets were fabricated by etching $Ti_3AlC_2$ MAX with HF, and then the L-Cysteine was used to functionalize the surface of MXene nanosheets. Subsequently, the L-Cysteine/MXene (fMX) hybrid material was characterized by FTIR, XRD, SEM, EDS and XPS. Then the anticorrosion properties of composite waterborne epoxy (WEP) coating containing fMX was investigated using electrochemical impedance spectroscopy and potentiodynamic polarization tests.

## 2. Experimental

### 2.1 Materials

Lithium fluoride (LiF), lithium chloride (LiCl) and L-Cysteine were purchased from Aladdin Chemicals Co., Ltd. (China). Hydrochloric acid (HCl, 37 wt.%) was supplied by Guangzhou Chemical Reagent Factory (China). MAX phase ($Ti_3AlC_2$, 99.7%) power was obtained from Nanjing Mission Advanced Materials Co., Ltd. (China). E51

were purchased from Guangzhou Dongfeng Chemicals Co., Ltd. (China) and its epoxy value was 0.51 mol/100g. Curing agent (BANCO901, active hydrogen equivalent is 248) was provided from B&C Chemicals Co., Ltd, China. Deionized water was prepared in our laboratory using an ultra-pure water machine (UPT-I-20L, ULUPURE, China).

**2.2 The preparation of MXene ($Ti_3C_2T_x$) nanosheets**

MXene ($Ti_3C_2T_x$) nanosheets were prepared by selective etching of Al layer from MAX ($Ti_3AlC_2$) powders. Firstly, 2.0 g of $Ti_3AlC_2$ powders were gradually added into mixture of 3.1 g of LiF powders and 40.0 mL of HCl solution (9 M). Then, the mixture was reacted for 48 hours at 38°C with continuous stirring. Subsequently, the mixture after reaction was centrifuged (3500 rpm for 5 min) and washed three times with 1 M HCl, 1 M LiCl and deionized water. Next, the precipitate was collected and re-dispersed in deionized water. After that, the solution was centrifuged for 10 min at 3500 rpm and 20 ℃. Finally, resulting MXene ($Ti_3C_2T_x$) nanosheets were collected.

**2.3 The modification of MXene**

0.5 g of L-Cysteine powder was dissolved in 50 mL of deionized water by stirring. Subsequently, 50.0 mL of MXene solution (10.0 mg/mL) was added into the solution under ultrasonic treatment (KQ-550VDE, Kunshan Ultrasound Instrument Co., Ltd., Kunshan, China) for 5 minutes and stirred at room temperature for 24 hours under nitrogen. After that, the solution was centrifuged and washed with deionized water. Finally, precipitate (fMX) was collected and re-dispersed in deionized water.

**2.4 The preparation of fMX/WEP nanocomposite coatings**

Firstly, the carbon steel sheets (120mm × 120mm × 1mm) were polished first by 180-grit and then 600-grit sandpaper and degreased with ethanol. 9.0 mL of fMX aqueous solution (1.80 mg/mL) was mixed with 5.8 g of waterborne hardener and 4.6 g of epoxy resin E51 by ultrasonic for 10 minutes. Then, the mixture was deposited on the as-prepared steel surface using an applicator with wet thickness of 90 μm. The fMX/WEP (0.2 wt.%) nanocomposite coatings were cured at room temperature for 48 h at 80 ℃ for 10 hours and the resulting thickness of dried coatings was 37 ± 4 μm. The blank WEP coatings without nanosheets and the MX/WEP with 0.2 wt.% pristine MXene nanosheets were prepared using the same procedure.

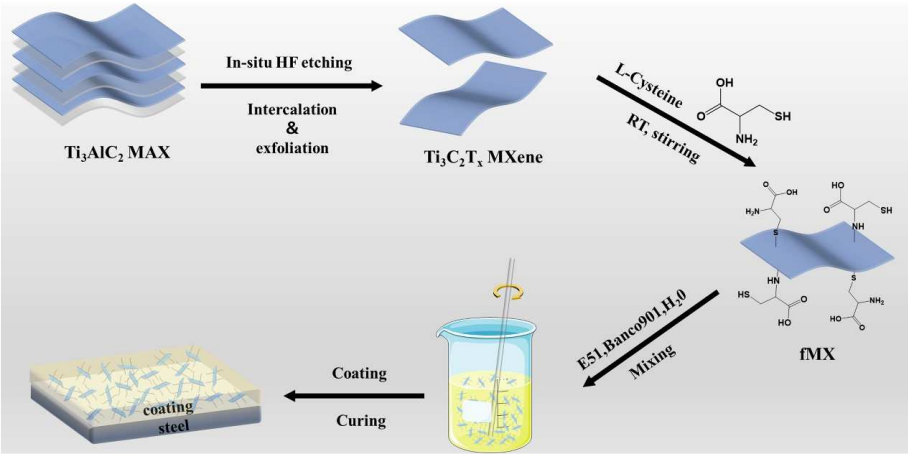


**Fig. 1.** The schematic graph of the preparation process of MXene ($Ti_3C_2T_x$), fMX and composite coating.

### 2.5 Characterization

X-ray diffraction (XRD) of $Ti_3AlC_2$, MXene and fMX was measured by Rigaku instrument, Japan with a $CuK_\alpha$ radiation ($\lambda$ = 0.15406 nm) source and the scanning rate was 10 °/min from 3°-60°. The MXene and fMX functional groups were analyzed by Fourier transform infrared (FTIR) spectra using VERTEX 70 spectrometer (Bruker Co., Germany). Morphology of MXene, fMX and the cross-section surfaces of coating was

investigated with a scanning electron microscope (SEM, HITACHI, Japan) and transmission electron microscope (TEM, JEM-2100, Japan). The energy dispersive spectroscopy (EDS) elemental mappings of pristine MXene and fMX were obtained by SEM. The chemical state of pristine MXene and fMX was characterised by X-ray photoelectron spectroscopy (XPS, Thermo fisher Scientific K-Alpha, USA).

**2.6 Electrochemical characterization**

Electrochemical impedance spectroscopy (EIS) and potentiodynamic polarization tests of three coatings were recorded by CHI660E electrochemical workstation (Chenhua, China). Three-electrode system was used in the electrochemical cell: (a) graphite as counter electrode; (b) saturated Ag/AgCl electrode as reference electrode and (c) the coated carbon steel as working electrode. The open circuit potential (OCP) must be in stable state before the EIS test. EIS was recorded in the frequency range of $10^5$ to $10^{-1}$ Hz at 10 mV amplitude. The electrochemical parameters were fitted and analyzed by ZSimpWin software. Potentiodynamic polarization curves were collected from -300 mV to +300 mV *vs.* OCP at a scan rate of 10 mV/s after coatings were immersed in 3.5 wt.% NaCl solution for 30 days.

**3. Results and discussion**

The schematic overview of the preparation process is shown in **Fig. 1**. The Al layer in $Ti_3AlC_2$ MAX phase was selectively in-situ etched by HF. Then, the single-layer MXene nanosheets was obtained through $Li^+$ ion intercalation and vibrating exfoliation. Next, surface functional modification of MXene with L-Cysteine was performed to

obtain MXene/L-Cysteine hybrid (fMX). Finally, MXene and fMX were added into epoxy resin and then applied on Q235 steel surface.

### 3.1 Basic characterization of fMX

#### 3.1.1 FTIR spectra

FTIR spectra of the pristine MXene and fMX are shown in **Fig. 2a**. It is obvious that the OH (3427 $cm^{-1}$), C-O (1630 $cm^{-1}$) and Ti-O (558 $cm^{-1}$) groups observed in all samples [36]. Compared with MXene, the new peaks in fMX samples appeared at 2928 $cm^{-1}$, 2858 $cm^{-1}$ and 1464 $cm^{-1}$, corresponding to symmetric and asymmetric vibrations of the C-H bonds, and the peaks at 1685 $cm^{-1}$ are attributed to the bending of N-H. The results presented here indicated that L-Cysteine has been successfully bounded on the MXene surface [37,38]. Both covalent bonds and non-covalent bonds can be formed, which was investigated by XPS (see Part 3.1.4).

#### 3.1.2 XRD

**Fig. 2b** shows the XRD curves of $Ti_3AlC_2$, MXene and fMX. The (104) peak of $Ti_3AlC_2$ at 39.0° completely disappeared indicating the Al layer was successfully etched [39,40]. Moreover, the (102) peak of $Ti_3AlC_2$ at 9.62° moved to a lower angle at 6.90°, and the d-spacing was increased from 9.19 Å to 12.80 Å demonstrating the single-layer MXene was prepared through $Li^+$ ions intercalations [41]. After being functionalized by L-Cysteine, the (002) peak of fMX moved to a much lower angle at 6.32°, and the d-spacing became 1.17 Å larger than the pristine MXene. It is a strong evidence that L-Cysteine functionalized on the surface of MXene so the interlayer spacing is expanded [38].

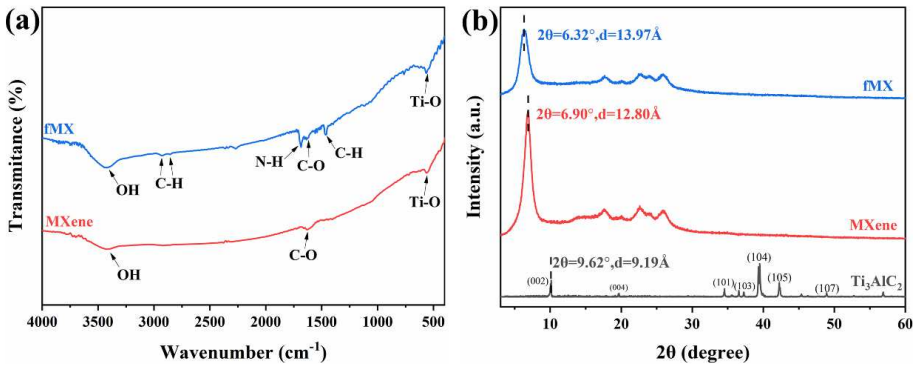


**Fig. 2.** (a) The FTIR spectra of MXene and fMX; (b)The XRD curves of $Ti_3AlC_2$, MXene and fMX.

### 3.1.3 Morphology

The morphology and microstructure of $Ti_3AlC_2$ MAX phase, MXene and fMX were observed by SEM and TEM. As shown in **Fig. 3a**, $Ti_3AlC_2$ MAX phase has closely stacked layered structure. After in-situ etched by HF for 48 h, the layers of MAX phase were separated from each other showing an accordion-like structure (**Fig. 3b**). It is indicating that the Al layer has been removed, which is consistent with XRD results. After intercalation and exfoliation, the single MXene flakes were obtained. The TEM image in **Fig. 3c** shows that MXene nanosheets were pretty thin and well-dispersed with no apparent stacked state. The SEM image of fMX is demonstrated in **Fig. 3d**, the surface of f-MX became rough, resulted from L-Cysteine functionalization.

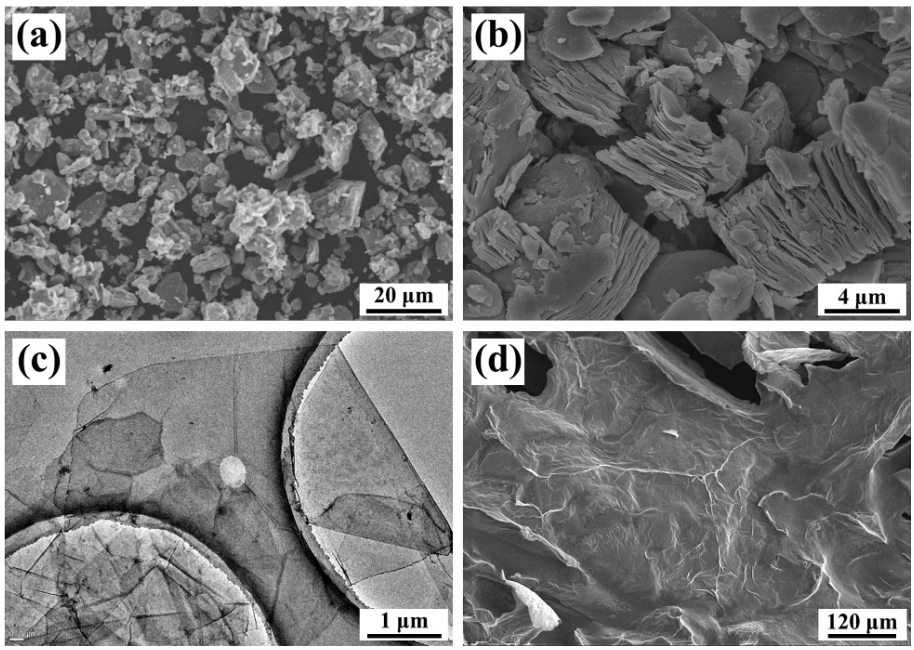


**Fig. 3.** SEM images of (a) MAX phase, (b) accordion-like MXene; (c) the TEM image of MXene nanosheets; (d) SEM images of fMX nanosheets

### 3.1.4 EDS mapping

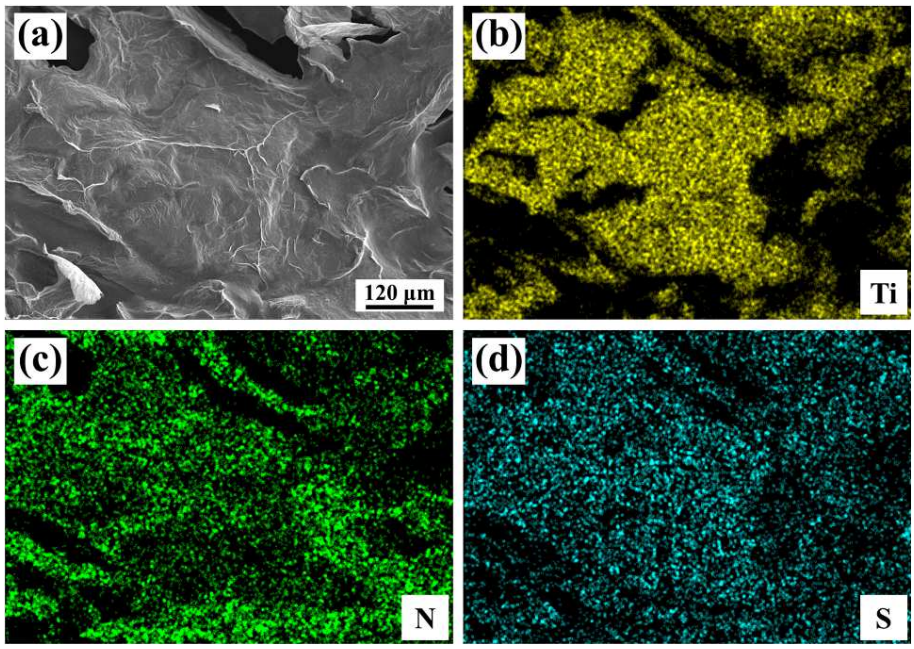


**Fig. 4.** The SEM-EDS mapping of fMX: (a)SEM image of fMX; (b) Ti, (c) N, (d) S distribution.

EDS mapping was used to confirm the distribution of L-Cysteine on fMX (**Fig. 4a**). The Ti element is characteristic for MXene ($Ti_3C_2T_x$) while the N and S elements indicate presence of L-Cysteine. As shown in **Fig. 4**, Ti, N and S elements were evenly distributed on fMX, proving that the MXene surface was well functionalized by L-Cysteine.

**3.1.4 XPS**

The wide scan XPS spectrum of pristine MXene and fMX is shown in **Fig. 5a**. C 1s (282.48 eV), F 1s (685.59 eV), O 1s (530.28 eV) and Ti 2p (456.01 eV) are present in both samples. Three new peaks at 400.42 eV, 227.08 eV and 163.29 eV coresponding to N 1s, S 2s and S 2p were observed only in fMX samples. As shown in **Fig. 5b**, the C1s of pristine MXene was deconvoluted into four peaks, which are C-Ti (282.46eV), C-C (284.8 eV), C-O (286.84 eV) and C=O (288.61 eV). C1s of fMX was consisted of C-Ti (281.96 eV), C-C (284.32 eV), C-N (284.93 eV), C-O (286.46 eV), C-S (287.08 eV) and C=O (288.42 eV). In the high resolution XPS spectra for N 1s (**Fig. 5c**) of fMX, there are three main peaks at 397.6 eV, 400.32 eV and 402.22 eV, which correspond to N-Ti, -NH- and N-H, respectively [38,42]. S 2p spectrum of fMX was broken down into two components (**Fig. 5d**). The low-energy side (162.24 and 162.81 eV) and the high energyside (163.82 and 165.17 eV) correspond to S-Ti and S-H respectively [43,44]. The result of XPS indicates that L-Cysteine is successfully grafted on the surface of MXene by forming N-Ti and S-Ti bond.

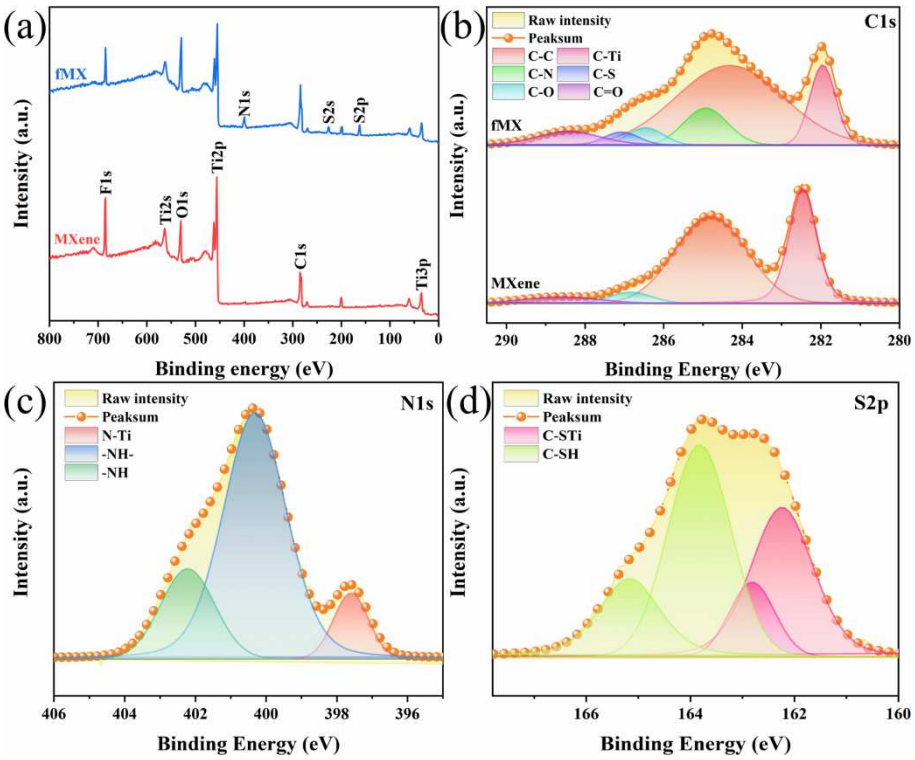


**Fig. 5.** (a) XPS spectra of pristine MXene and fMX; (b) C 1s spectra of pristine MXene and fMX; (c) N 1s spectrum of fMX; (d)S 2p spectrum of fMX.

### 3.2 Characterization of fMX/WEP nanocomposite coatings

#### 3.2.1 Morphology of composite coatings

The dispersion of nanosheets in polymer matrix is an important factor affecting the anti-corrosion performance of coatings. The fractured surface of three coatings was characterized by SEM and is shown in **Fig. 6**. It can be observed from **Fig. 6a-b** that the fracture surface of blank WEP is smooth with obvious long cracks and holes. As shown in **Fig. 6c-d**, with the addition of MXene nanosheets, the fractured surface of MX/WEP became rough and the cracks were disorderly distributed. Moreover, some agglomerated MXene can also be observed, indicating that unmodified MXene would result in uneven dispersion of MXene in epoxy matrix. However, since functionalized with L-Cysteine fMX have more affinity to WEP than MXene, fMX makes the section

of fMX/WEP rough but the cracks are relatively uniform (**Fig. 6e-f**). The above results indicate that the dispersibility of fMX in the epoxy matrix is superior to that of MXene, which effectively improves the barrier performance of the epoxy coating to corrosive media.

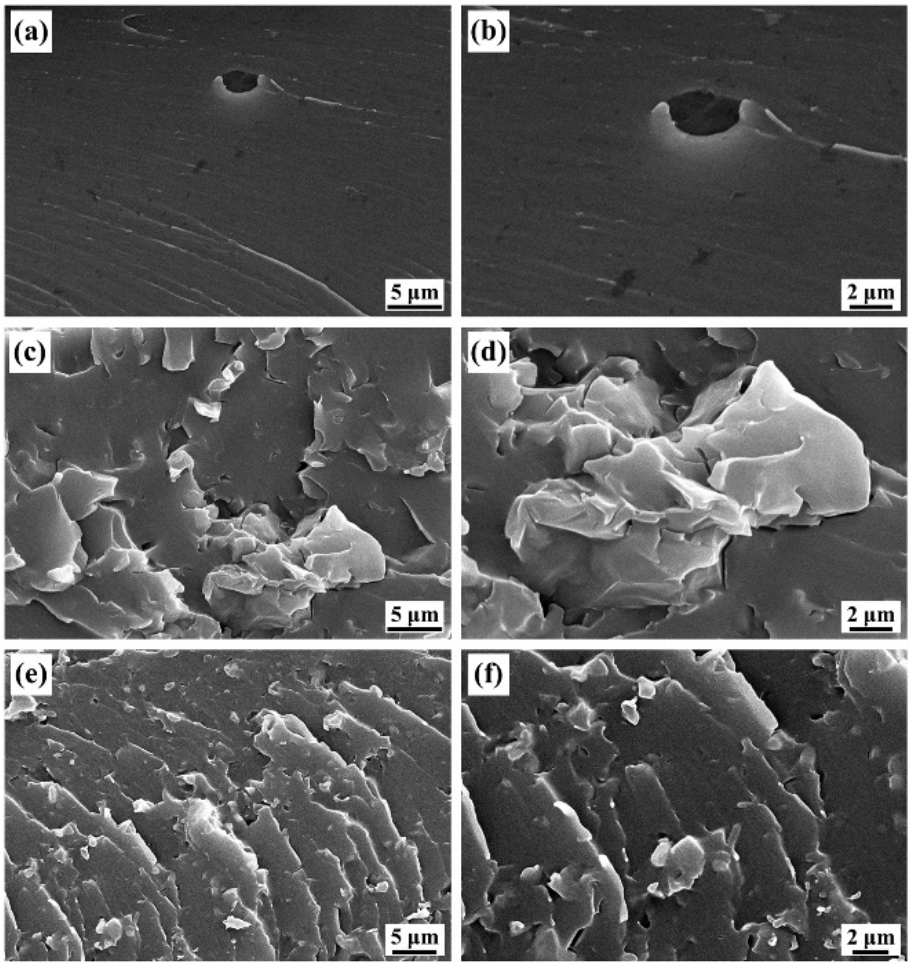


**Fig. 6.** SEM images of fractured surface of (a-b) blank WEP; (c-d) MX/WEP; (e-f) fMX/WEP.

### 3.3 Corrosion protection property measurement

#### 3.3.1 Electrochemical impedance spectroscopy (EIS)

Electrochemical impedance spectroscopy (EIS) test is an important method to study the long-term anti-corrosion performance of coatings [45,46]. EIS tests were conducted on

the coatings immersed in 3.5 wt.% NaCl solution for 1, 10, 20, and 30 days, respectively, and plotted as Nyquist diagrams and Bode diagrams. At the same time, the EIS data were analyzed through ZSimpWin software and fitted by the equivalent electric circuits (EECs).

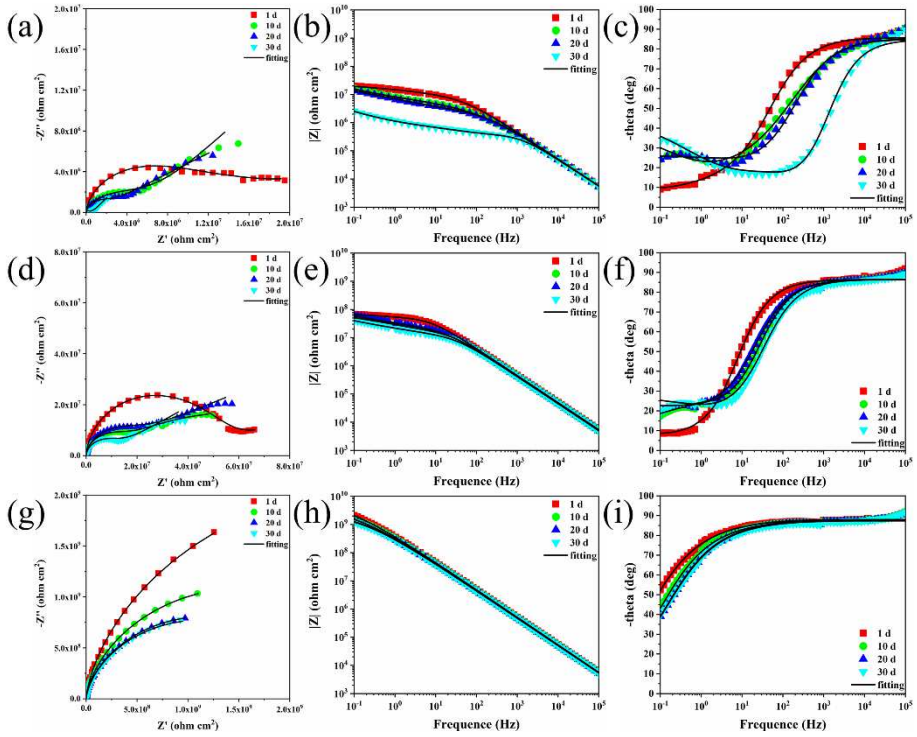


**Fig. 7.** Nyquist and Bode plots of blank WEP (a, b, c); MX/WEP (d, e, f); fMX/WEP (g, h, i) immersed in 3.5 wt.% NaCl solution.

The Nyquist and Bode plots were shown in **Fig. 7**. For blank WEP the diameters at high frequencies in **Fig. 7a** and the modulus at lowest frequency of **Fig. 7b** decreased sharply after being immersed for 30 days, while the phase angle in **Fig. 7c** moved to a higher frequency with the increase of immersing time. These results show that the electrolyte solution can easily reach the surface of the metal substrate and form a mass transferring layer, which is mainly due to blank WEP has many micro-pores and defects after curing. The diameters at high frequencies in Nyquist plot (**Fig. 7d**) and the lowest-

frequency modulus in Bode plot (**Fig. 7e**) both had slower descending trend than blank WEP when MXene was added into epoxy coating owing to the excellent barrier performance of Mxene nanoplates. Warburg diffusion slope appeared after 10 days immersion, which may be due to the gap between Mxene nanoplates and the epoxy. After using L-Cysteine modified MXene as fillers for WEP, the EIS performance of fMX/WEP improved significantly with negligible changes in low-frequency impedance modulus after 30 days of immersion in 3.5 wt.% NaCl solution.

In order to compare the corrosion behavior of three coatings during immersion, the impedance modulus at lowest frequency ($|Z_{0.1Hz}|$) and breakpoint frequency at -45° phase angle ($f_b$) were shown at **Fig. 8**. The impedance modulus at lowest frequency ($|Z_{0.1Hz}|$) can reflect the protective performance of the coating [47]. As shown in **Fig. 8a**, the $|Z_{0.1Hz}|$ of blank WEP decreased from $1.98\times10^7$ to $2.54\times10^6$ $\Omega\cdot cm^2$ after 30 days of immersion, while the $|Z_{0.1Hz}|$ of MX/WEP decreased from $6.69\times10^7$ to $4.12\times10^7$ $\Omega\cdot cm^2$ after adding MXene, this is because the addition of MXene nano-fillers provides a "maze effect" on WEP coatings making it more difficult for electrolyte to penetrate through coatings. With the addition of fMX, the $|Z_{0.1Hz}|$ was greatly improved, which is two orders of magnitude larger than MX/WEP and three orders of magnitude as for blank WEP. It is indicating that fMX/WEP has the best corrosion resistance of the three composite coatings.

Breakpoint frequency at -45° phase angle ($f_b$) is in proportion to the coating defect area [48]; therefore, the coating with low $f_b$ has better corrosion resistance. As shown in **Fig. 8**, each period (1, 10, 20, and 30 days) of blank WEP has the largest $f_b$ value

among the three coatings. As the immersion time increases, the $f_b$ of blank WEP increases most obviously, from 37.66 Hz to 1260.12 Hz, which is mainly due to the accumulation of corrosion products resulted in serious delamination between the coating and metal substrate. The $f_b$ of MX/WEP varies from 7.09 Hz to 23.48 Hz, which is smaller than that of blank WEP and has a slight change. The addition of MXene can effectively slow down the penetration of corrosive media. The $f_b$ value of fMX/WEP appears after 10 days of immersion and very stable (from 0.11 Hz to 0.14 Hz) during 30 days showing that the addition of fMX effectively reduces the porosity of the coating.

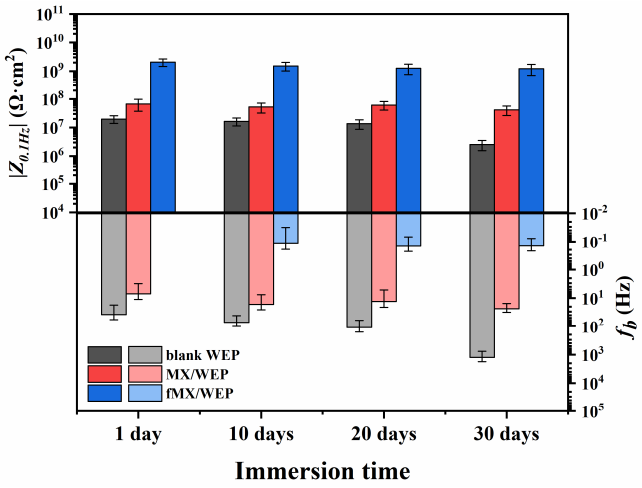


**Fig. 8.** Impedance modulus at 0.1 Hz frequencies ($|Z_{0.1Hz}|$) and breakpoint frequencies at -45° phase angle ($f_b$) of blank WEP, MX/WEP and fMX/WEP coatings after 1 day, 10 days, 20 days and 30 days of exposure to 3.5 wt.% NaCl aqueous solution.

We used the equivalent electrical circuits (EECs) in **Fig. 9a** to fit EIS data by ZSimpWin software and listed the circuit parameters in Table S1. Model A is usually used to simulate the coating/metal interface when the penetration of the electrolyte solution reaches its saturation in coating. In this model, $R_s$ represents the solution resistance; $R_{po}$, $R_{ct}$ are the pore resistance and the charge transfer resistance, respectively,

$R_{po}$ is related to the pore area of coating surface and interface blistering area and decreases with the increase of porosity and blistering rate; $CPE_c$ and $CPE_{dl}$ are coated non-ideal capacitors and double-layer non-ideal capacitors. Model A is suitable for fMX/WEP. The coating was destroyed and degraded as the electrolyte continues to penetrate, and the concentration gradient existing in the coating also disappears. Furthermore, if corrosion reaction in the interface area between the coating and the metal substrate accelerates, a new diffusion layer appears. Model B is set for coating in this period, where $Z_w$ represents Warburg impedance, we use Model B to fit blank WEP and MX/WEP.

$R_{po}$ is an important indicator for evaluating coating density and porosity. As shown in **Fig. 9b**, the $R_{po}$ value of the blank WEP decreases from $3.32\times10^6$ to $3.65\times10^5$ $\Omega\cdot cm^2$ after 30 days of immersion, which indicates that the blank WEP lost its ability to prevent penetration of corrosive media. After adding MXene, the $R_{po}$ value of MX/WEP improved (from $1.46\times10^7$ to $7.26\times10^6$ $\Omega\cdot cm^2$). It is attributed to 2D structure and large surface of MXene. The initial $R_{po}$ value of fMX/WEP was $1.44\times10^8$ $\Omega\cdot cm^2$ and then decreased to $6.51\times10^7$ $\Omega\cdot cm^2$ and is about two orders of magnitude larger than that of blank WEP at the same time, which shows fMX/WEP has higher density and lower porosity.

$R_{ct}$ is inversely proportional to the metal corrosion rate [49]. It can be clearly seen from **Fig. 9c** that the $R_{ct}$ of the three coatings decreases with the increase of immersion time. The order of $R_{ct}$ value from high to low is: fMX/WEP, MX/WEP, blank WEP, and the $R_{ct}$ value of fMX/WEP is at least 2 orders of magnitude larger than blank WEP

showing that the corrosion resistance of epoxy coating is greatly improved after adding fMX nanosheets.

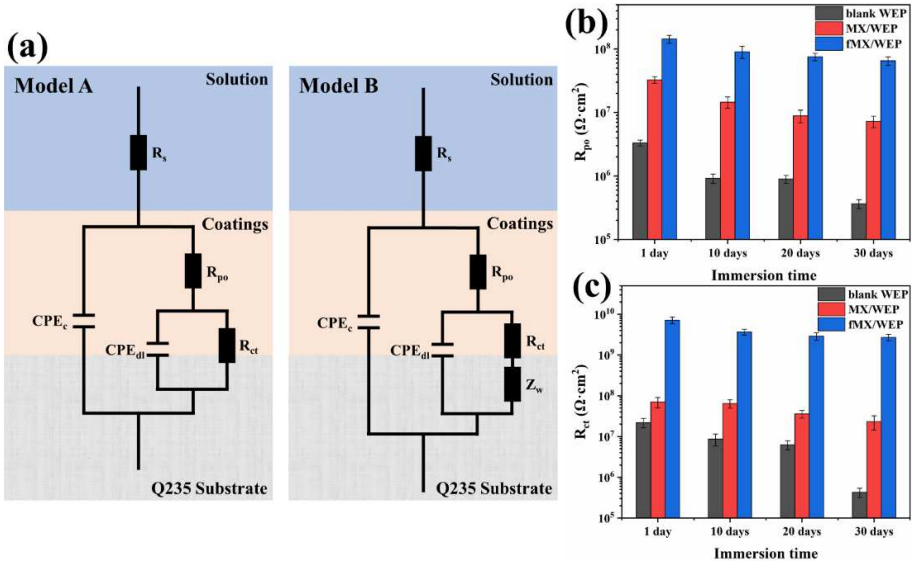


**Fig. 9.** (a) The equivalent electrical circuits (EEC) and the electrical parameters (b) $R_{po}$ and (c) $R_{ct}$

### 3.3.2 The potentiodynamic polarization (PD) test

In order to evaluate the anti-corrosion performance of the coating, the coatings were subjected to potentiodynamic polarization test after 30 days of immersion in 3.5% NaCl solution (**Fig. 10**). Further, we used Tafel extrapolation, Stern-Geary equation and Faraday's law formula to calculate the corrosion potential ($E_{corr}$), corrosion current density ($I_{corr}$), polarization resistance ($R_p$), anode ($b_a$) and cathode ($b_c$) slopes and corrosion rate ($CR$) [50,51] (see Table 1).

Generally, the coating with higher $E_{corr}$ and $R_p$, lower $I_{corr}$ has better corrosion resistance [7]. The $E_{corr}$ of MX/WEP and fMX/WEP are -224.21 mV and -220.7 mV, which are significantly higher than the blank WEP (-571.84 mV). The $I_{corr}$ of fMX/WEP is $1.22\times10^{-10}$ A/cm$^2$, which is one order of magnitude lower than for MX/WEP

($5.32\times10^{-9}$ A/cm$^2$) and two order of magnitude lower than for blank WEP ($4.74\times10^{-8}$ A/cm$^2$). In addition, fMX/WEP has the largest polarization resistance ($3.44\times10^{8}$ Ω·cm$^2$) and the smallest corrosion rate ($7.95\times10^{-6}$ mpy). It is three orders of magnitude larger and three orders of magnitude smaller than pure epoxy coating ($8.77\times10^{5}$ Ω·cm$^2$ and $3.08\times10^{-3}$ mpy), respectively, indicating that fMX/WEP has the best anti-corrosion performance among the three coatings.

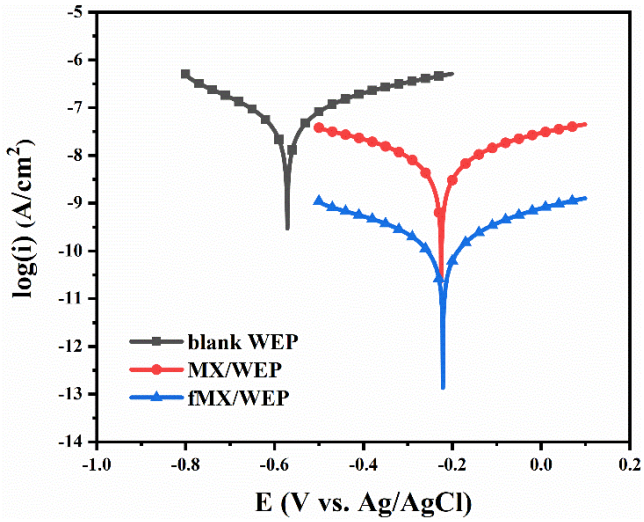


**Fig. 10.** Potentiodynamic polarization curves of coatings after 30 days of immersion in 3.5 wt.% NaCl aqueous solution.

**Table 1.** Tafel extrapolation results obtained from Fig. 10.

| Sample | $E_{corr}$ (mV) | $I_{corr}$ (A/cm$^2$) | $R_p$ (Ω·cm$^2$) | $b_a$ (mV/dec) | $b_c$ (mV/dec) | $CR$ (mpy) |
|---|---|---|---|---|---|---|
| blank/WEP | -571.84 | $4.74\times10^{-8}$ | $8.77\times10^{5}$ | 182.31 | -201.16 | $3.08\times10^{-3}$ |
| MX/WEP | -224.21 | $5.32\times10^{-9}$ | $8.14\times10^{6}$ | 200.24 | -198.25 | $3.46\times10^{-4}$ |
| fMX/WEP | -220.7 | $1.22\times10^{-10}$ | $3.44\times10^{8}$ | 198.96 | -188.89 | $7.95\times10^{-6}$ |

Above results are consistent with the previous electrochemical impedance spectroscopy (EIS) test results, which shows that although the addition of MXene gives

the WEP coating good barrier properties, its improvement is limited due to the poor dispersion of the MXene nanosheets in the resin matrix. After using L-Cysteine to modify MXene, fMX has good dispersibility in the coating and improves the compactness of the coating, which makes it difficult for the corrosive medium to pass through the coating and react with the metal substrate.

### 3.3.3 Characterization of corrosion layers on the surface of substrate

After immersing in 3.5 wt.% NaCl solution for 30 days, the steel substrates with the upper coating removed, and was characterized by SEM and EDS. As shown in the **Fig. 11**, the surface of the substrate coated with blank WEP and MX/WEP produced a large amount of corrosion products after the corrosion test. EDS can analyze the penetration degree of corrosive media on metal substrates [52,53]. It can be seen from the EDS results that the corrosion surfaces of blank WEP and MX/WEP revealed a large amount of O (19.733wt.% and 18.696 wt.%, respectively) and Cl (3.346 wt.% and 9.904 wt.%, respectively), which indicates that the surface of the substrate is severely corroded. However, the surface of the substrate coated with fMX/WEP is well preserved and only a small amount of O (0.899 wt.%) and Cl (0.012 wt.%) appeared.

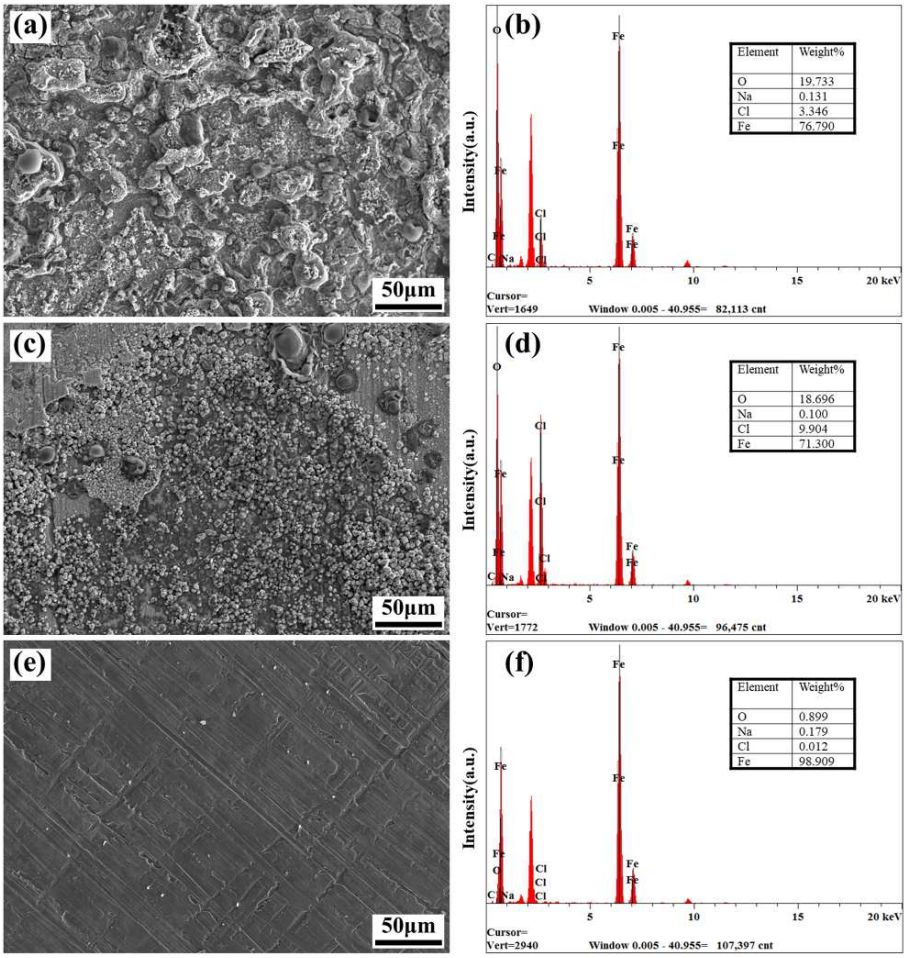


**Fig 11.** SEM images and EDS spectra of substrate coated by (a, b) blank WEP; (c, d) MX/WEP; (g, h) fMX/WEP after immersion in 3.5 wt.% NaCl aqueous solution for 30 days.

### 3.3.4 The corrosion protection mechanism of epoxy coating

**Fig. 12** demonstrates the possible mechanism of MX/WEP and fMX/WEP protection. The addtion of MXene nanosheets with high surface area enhances the barrier performance of epoxy coating; however, the poor dispersion and compatibility of MXene in the epoxy matrix limit the reinforcement of MXene. L-Cysteine surface modification of MXene improves the dispersion of fMX in epoxy coating, which lengthens the diffusion path and increases the difficulty of the penetration of corrosive media.

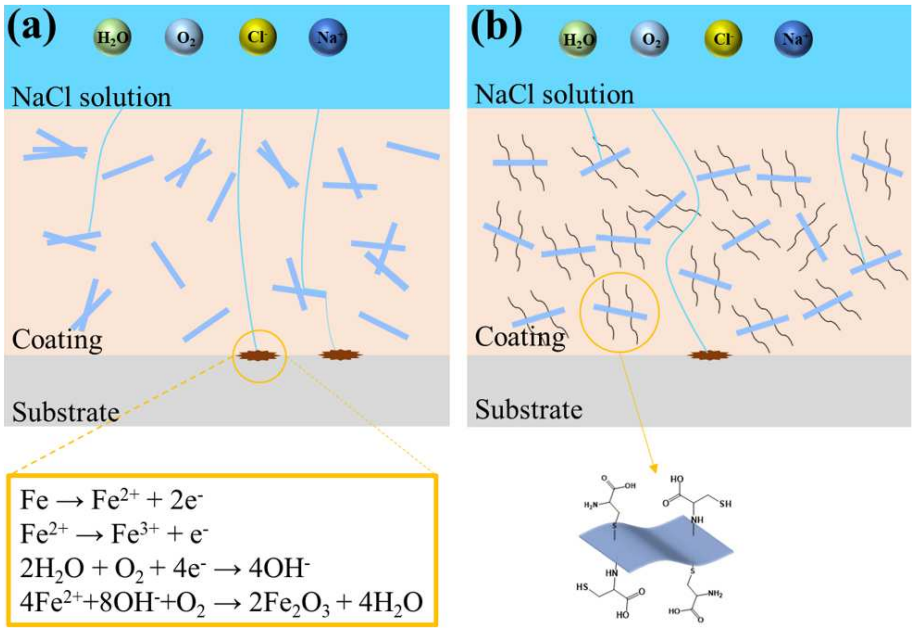


**Fig 12.** Schematic representation of corrosion process of (a) MX/WEP and (b) fMX/WEP coatings.

## 4. Conclusions

In this article, the functionalized MXene (fMX) hybrid material was successfully prepared by the covalent reaction of L-Cysteine and MXene surface, which was confirmed by FTIR, XRD, SEM, EDS mapping and XPS. Then, we introduced fMX into epoxy coatings and used EIS test and potentiodynamic polarization test to characterize the anti-corrosion performance of fMX/WEP. The SEM of coatings surface revealed that the dispersion performance of fMX in waterborne epoxy coatings is significantly better than that of MXene. Moreover, the electrochemical test results showed that fMX/WEP has highest low frequency impedance ($1.21\times10^{9}$ $\Omega\cdot cm^{2}$) and smallest corrosion rate ($7.95\times10^{-6}$ mpy), which are 3 orders of magnitude higher and 3 orders of magnitude lower than that of blank WEP. SEM and EDS spectra also showed that fMX/WEP effectively slows down the corrosion rate of metal substrates compared

to other two coatings. This is mainly due to: (1) good dispersion performance of fMX in epoxy matrix; (2) excellent barrier properties of MXene nanosheets with high aspect ratio.

**Acknowledgements**

This work was supported by the National Natural Science Foundation of China (Grant No. 51908031). Haowei Huang thanks the China Scholarship Council for a graduate fellowship (201906150013). Y. C. acknowledges the support from Guangdong Special Support Program (Grant No. 2017TX04N371).

**Reference**

[1] L. Hao, S. Zhang, J. Dong, W. Ke, Atmospheric corrosion resistance of MnCuP weathering steel in simulated environments, Corros. Sci. 53 (2011) 4187–4192. https://doi.org/10.1016/j.corsci.2011.08.028.

[2] D. Borisova, H. Möhwald, D.G. Shchukin, Mesoporous Silica Nanoparticles for Active Corrosion Protection, ACS Nano. 5 (2011) 1939–1946. https://doi.org/10.1021/nn102871v.

[3] D. Borisova, H. Möhwald, D.G. Shchukin, Influence of embedded nanocontainers on the efficiency of active anticorrosive coatings for aluminum alloys part II: influence of nanocontainer position, ACS Appl. Mater. Interfaces. 5 (2013) 80–87. https://doi.org/10.1021/am302141y.

[4] G.P. Bierwagen, Reflections on corrosion control by organic coatings, Prog. Org. Coat. 28 (1996) 43–48. https://doi.org/10.1016/0300-9440(95)00588-9.

[5] Z. Zheng, M. Schenderlein, X. Huang, N.J. Brownbill, F. Blanc, D. Shchukin, Influence of functionalization of nanocontainers on self-healing anticorrosive coatings, ACS Appl. Mater. Interfaces. 7 (2015) 22756–22766. https://doi.org/10.1021/acsami.5b08028.

[6] D. Li, F. Wang, X. Yu, J. Wang, Q. Liu, P. Yang, Y. He, Y. Wang, M. Zhang, Anticorrosion organic coating with layered double hydroxide loaded with corrosion inhibitor of tungstate, Prog. Org. Coat. 71 (2011) 302–309. https://doi.org/10.1016/j.porgcoat.2011.03.023.

[7] S. Zheng, D.A. Bellido-Aguilar, J. Hu, Y. Huang, X. Zhao, Z. Wang, X. Zeng, Q. Zhang, Z. Chen, Waterborne bio-based epoxy coatings for the corrosion protection of metallic substrates, Prog. Org. Coat. 136 (2019) 105265. https://doi.org/10.1016/j.porgcoat.2019.105265.

[8] H. Zheng, Y. Shao, Y. Wang, G. Meng, B. Liu, Reinforcing the corrosion protection property of epoxy coating by using graphene oxide–poly(urea–formaldehyde) composites, Corros. Sci. 123 (2017) 267–277. https://doi.org/10.1016/j.corsci.2017.04.019.

[9] C. Liang, P. Song, H. Gu, C. Ma, Y. Guo, H. Zhang, X. Xu, Q. Zhang, J. Gu, Nanopolydopamine coupled fluorescent nanozinc oxide reinforced epoxy nanocomposites, Compos. Part Appl. Sci. Manuf. 102 (2017) 126–136. https://doi.org/10.1016/j.compositesa.2017.07.030.

[10] Y. Xia, N. Zhang, Z. Zhou, C. Chen, Y. Wu, F. Zhong, Y. Lv, Y. He, Incorporating SiO2 functionalized g-C3N4 sheets to enhance anticorrosion performance of

waterborne epoxy, Prog. Org. Coat. 147 (2020) 105768. https://doi.org/10.1016/j.porgcoat.2020.105768.

[11] X. Zhu, Z. Ni, L. Dong, Z. Yang, L. Cheng, X. Zhou, Y. Xing, J. Wen, M. Chen, In-situ modulation of interactions between polyaniline and graphene oxide films to develop waterborne epoxy anticorrosion coatings, Prog. Org. Coat. 133 (2019) 106–116. https://doi.org/10.1016/j.porgcoat.2019.04.016.

[12] Y. Wu, J. Yu, W. Zhao, C. Wang, B. Wu, G. Lu, Investigating the anti-corrosion behaviors of the waterborne epoxy composite coatings with barrier and inhibition roles on mild steel, Prog. Org. Coat. 133 (2019) 8–18. https://doi.org/10.1016/j.porgcoat.2019.04.028.

[13] C. Chen, Y. He, G. Xiao, F. Zhong, Y. Xia, Y. Wu, Graphic C3N4-assisted dispersion of graphene to improve the corrosion resistance of waterborne epoxy coating, Prog. Org. Coat. 139 (2020) 105448. https://doi.org/10.1016/j.porgcoat.2019.105448.

[14] C. Huang, Q. Cheng, Learning from nacre: Constructing polymer nanocomposites, Compos. Sci. Technol. 150 (2017) 141–166. https://doi.org/10.1016/j.compscitech.2017.07.021.

[15] H. Huang, X. Sheng, Y. Tian, L. Zhang, Y. Chen, X. Zhang, Two-Dimensional Nanomaterials for Anticorrosive Polymeric Coatings: A Review, Ind. Eng. Chem. Res. 59 (2020) 15424–15446. https://doi.org/10.1021/acs.iecr.0c02876.

[16] S. Pourhashem, M.R. Vaezi, A. Rashidi, M.R. Bagherzadeh, Exploring corrosion protection properties of solvent based epoxy-graphene oxide nanocomposite

coatings on mild steel, Corros. Sci. 115 (2017) 78–92. https://doi.org/10.1016/j.corsci.2016.11.008.

[17] P. Song, B. Liu, C. Liang, K. Ruan, H. Qiu, Z. Ma, Y. Guo, J. Gu, Lightweight, Flexible Cellulose-Derived Carbon Aerogel@Reduced Graphene Oxide/PDMS Composites with Outstanding EMI Shielding Performances and Excellent Thermal Conductivities, Nano-Micro Lett. 13 (2021) 91. https://doi.org/10.1007/s40820-021-00624-4.

[18] X. Ji, Y. Xu, W. Zhang, L. Cui, J. Liu, Review of functionalization, structure and properties of graphene/polymer composite fibers, Compos. Part Appl. Sci. Manuf. 87 (2016) 29–45. https://doi.org/10.1016/j.compositesa.2016.04.011.

[19] B. Ramezanzadeh, G. Bahlakeh, M.H. Mohamadzadeh Moghadam, R. Miraftab, Impact of size-controlled p-phenylenediamine (PPDA)-functionalized graphene oxide nanosheets on the GO-PPDA/Epoxy anti-corrosion, interfacial interactions and mechanical properties enhancement: Experimental and quantum mechanics investigations, Chem. Eng. J. 335 (2018) 737–755. https://doi.org/10.1016/j.cej.2017.11.019.

[20] S. Pourhashem, A. Rashidi, M.R. Vaezi, M.R. Bagherzadeh, Excellent corrosion protection performance of epoxy composite coatings filled with amino-silane functionalized graphene oxide, Surf. Coat. Technol. 317 (2017) 1–9. https://doi.org/10.1016/j.surfcoat.2017.03.050.

[21] M. Naguib, M. Kurtoglu, V. Presser, J. Lu, J. Niu, M. Heon, L. Hultman, Y. Gogotsi, M.W. Barsoum, Two-Dimensional Nanocrystals Produced by Exfoliation of

Ti3AlC2, Adv. Mater. 23 (2011) 4248–4253. https://doi.org/10.1002/adma.201102306.

[22] P. Song, B. Liu, H. Qiu, X. Shi, D. Cao, J. Gu, MXenes for polymer matrix electromagnetic interference shielding composites: A review, Compos. Commun. 24 (2021) 100653. https://doi.org/10.1016/j.coco.2021.100653.

[23] M. Sajid, MXenes: Are they emerging materials for analytical chemistry applications? – A review, Anal. Chim. Acta. 1143 (2021) 267–280. https://doi.org/10.1016/j.aca.2020.08.063.

[24] L. Guo, Z. Zhang, M. Li, R. Kang, Y. Chen, G. Song, S.-T. Han, C.-T. Lin, N. Jiang, J. Yu, Extremely high thermal conductivity of carbon fiber/epoxy with synergistic effect of MXenes by freeze-drying, Compos. Commun. 19 (2020) 134–141. https://doi.org/10.1016/j.coco.2020.03.009.

[25] L. Wang, H. Qiu, P. Song, Y. Zhang, Y. Lu, C. Liang, J. Kong, L. Chen, J. Gu, 3D Ti3C2Tx MXene/C hybrid foam/epoxy nanocomposites with superior electromagnetic interference shielding performances and robust mechanical properties, Compos. Part Appl. Sci. Manuf. 123 (2019) 293–300. https://doi.org/10.1016/j.compositesa.2019.05.030.

[26] H. Yan, W. Li, H. Li, X. Fan, M. Zhu, Ti3C2 MXene nanosheets toward high-performance corrosion inhibitor for epoxy coating, Prog. Org. Coat. 135 (2019) 156–167. https://doi.org/10.1016/j.porgcoat.2019.06.013.

[27] H. Yan, M. Cai, W. Li, X. Fan, M. Zhu, Amino-functionalized Ti3C2T with anti-corrosive/wear function for waterborne epoxy coating, J. Mater. Sci. Technol. 54 (2020) 144–159. https://doi.org/10.1016/j.jmst.2020.05.002.

[28] C. Liu, P. Du, H. Zhao, L. Wang, Synthesis of l-Histidine-Attached Graphene Nanomaterials and Their Application for Steel Protection, ACS Appl. Nano Mater. 1 (2018) 1385–1395. https://doi.org/10.1021/acsanm.8b00149.

[29] X. Zhou, H. Huang, R. Zhu, X. Sheng, D. Xie, Y. Mei, Facile modification of graphene oxide with Lysine for improving anti-corrosion performances of water-borne epoxy coatings, Prog. Org. Coat. 136 (2019) 105200. https://doi.org/10.1016/j.porgcoat.2019.06.046.

[30] F. Elmi, A. Gharakhani, S. Ghasemi, H. Alinezhad, Self-assemble l-glycine and l-cysteine/polydopamine nanohybrid films coated on 304 stainless steel for corrosion study in sterile seawater, Prog. Org. Coat. 119 (2018) 127–137. https://doi.org/10.1016/j.porgcoat.2018.01.010.

[31] F. Elmi, E. Valipour, S. Ghasemi, Synthesis of anticorrosion nanohybrid films based on bioinspired dopamine, L-cys/CNT@PDA through self-assembly on 304 stainless steel in 3.5% NaCl, Bioelectrochemistry. 126 (2019) 79–85. https://doi.org/10.1016/j.bioelechem.2018.11.012.

[32] J. Fu, S. Li, Y. Wang, L. Cao, L. Lu, Computational and electrochemical studies of some amino acid compounds as corrosion inhibitors for mild steel in hydrochloric acid solution, J. Mater. Sci. 45 (2010) 6255–6265. https://doi.org/10.1007/s10853-010-4720-0.

[33] A. Yadav, R. Kumar, B. Sahoo, Graphene Oxide Coatings on Amino Acid Modified Fe Surfaces for Corrosion Inhibition, ACS Appl. Nano Mater. 3 (2020) 3540–3557. https://doi.org/10.1021/acsanm.0c00243.

[34] T. Wang, J. Wang, Y. Wu, The inhibition effect and mechanism of l-cysteine on the corrosion of bronze covered with a CuCl patina, Corros. Sci. 97 (2015) 89–99. https://doi.org/10.1016/j.corsci.2015.04.018.

[35] T. Stimpfling, P. Vialat, H. Hintze-Bruening, P. Keil, V. Shkirskiy, P. Volovitch, K. Ogle, F. Leroux, Amino Acid Interleaved Layered Double Hydroxides as Promising Hybrid Materials for AA2024 Corrosion Inhibition, Eur. J. Inorg. Chem. 2016 (2016) 2006–2016. https://doi.org/10.1002/ejic.201501161.

[36] Z. Ma, S. Kang, J. Ma, L. Shao, Y. Zhang, C. Liu, A. Wei, X. Xiang, L. Wei, J. Gu, Ultraflexible and Mechanically Strong Double-Layered Aramid Nanofiber–Ti3C2Tx MXene/Silver Nanowire Nanocomposite Papers for High-Performance Electromagnetic Interference Shielding, ACS Nano. 14 (2020) 8368–8382. https://doi.org/10.1021/acsnano.0c02401.

[37] Riazi H., Anayee M., Hantanasirisakul K., Shamsabadi A.A., Anasori B., Gogotsi Y., Soroush M., Surface Modification of a MXene by an Aminosilane Coupling Agent, Adv. Mater. Interfaces. 7 (2020) 1902008. https://doi.org/10.1002/admi.201902008.

[38] C. Chen, M. Boota, P. Urbankowski, B. Anasori, L. Miao, J. Jiang, Y. Gogotsi, Effect of glycine functionalization of 2D titanium carbide (MXene) on charge

storage, J. Mater. Chem. A. 6 (2018) 4617–4622. https://doi.org/10.1039/c7ta11347a.

[39] P. Song, H. Qiu, L. Wang, X. Liu, Y. Zhang, J. Zhang, J. Kong, J. Gu, Honeycomb structural rGO-MXene/epoxy nanocomposites for superior electromagnetic interference shielding performance, Sustain. Mater. Technol. 24 (2020) e00153. https://doi.org/10.1016/j.susmat.2020.e00153.

[40] Y. Zhang, L. Wang, J. Zhang, P. Song, Z. Xiao, C. Liang, H. Qiu, J. Kong, J. Gu, Fabrication and investigation on the ultra-thin and flexible Ti3C2Tx/co-doped polyaniline electromagnetic interference shielding composite films, Compos. Sci. Technol. 183 (2019) 107833. https://doi.org/10.1016/j.compscitech.2019.107833.

[41] L. Wang, P. Song, C.-T. Lin, J. Kong, J. Gu, 3D Shapeable, Superior Electrically Conductive Cellulose Nanofibers/$Ti_3C_2T_x$ MXene Aerogels/Epoxy Nanocomposites for Promising EMI Shielding, Research. 2020 (2020) 1–12. https://doi.org/10.34133/2020/4093732.

[42] H. Yue, H. Sun, T. Peng, B. Liu, Y. Xie, Evolution of structure and functional groups in the functionalization of graphene oxide with L-cysteine, J. Mol. Struct. 1163 (2018) 449–454. https://doi.org/10.1016/j.molstruc.2018.02.111.

[43] A. Jürgensen, H. Raschke, N. Esser, R. Hergenröder, An in situ XPS study of L-cysteine co-adsorbed with water on polycrystalline copper and gold, Appl. Surf. Sci. 435 (2018) 870–879. https://doi.org/10.1016/j.apsusc.2017.11.150.

[44] D. Gonbeau, C. Guimon, G. Pfister-Guillouzo, A. Levasseur, G. Meunier, R. Dormoy, XPS study of thin films of titanium oxysulfides, Surf. Sci. 254 (1991) 81–89. https://doi.org/10.1016/0039-6028(91)90640-e.

[45] F. Mansfeld, Electrochemical impedance spectroscopy (EIS) as a new tool for investigating methods of corrosion protection, Electrochimica Acta. 35 (1990) 1533–1544. https://doi.org/10.1016/0013-4686(90)80007-b.

[46] X. Liu, J. Xiong, Y. Lv, Y. Zuo, Study on corrosion electrochemical behavior of several different coating systems by EIS, Prog. Org. Coat. 64 (2009) 497–503. https://doi.org/10.1016/j.porgcoat.2008.08.012.

[47] S. Qiu, C. Chen, W. Zheng, W. Li, H. Zhao, L. Wang, Long-term corrosion protection of mild steel by epoxy coating containing self-doped polyaniline nanofiber, Synth. Met. 229 (2017) 39–46. https://doi.org/10.1016/j.synthmet.2017.05.004.

[48] X.P. Liu, T.L. Zheng, J.P. Xiong, Corrosion Resistance of Polyurea Polyaspartic Ester Coating in 3.5%NaCl by EIS, Int J Electrochem Sci. 8 (2013) 8.

[49] S. González, F. Cáceres, V. Fox, R.M. Souto, Resistance of metallic substrates protected by an organic coating containing aluminum powder, Prog. Org. Coat. 46 (2003) 317–323. https://doi.org/10.1016/s0300-9440(03)00021-3.

[50] H. Huang, X. Huang, Y. Xie, Y. Tian, X. Jiang, X. Zhang, Fabrication of h-BN-rGO@PDA nanohybrids for composite coatings with enhanced anticorrosion performance, Prog. Org. Coat. 130 (2019) 124–131. https://doi.org/10.1016/j.porgcoat.2019.01.059.

[51] E. McCafferty, Validation of corrosion rates measured by the Tafel extrapolation method, Corros. Sci. 47 (2005) 3202–3215. https://doi.org/10.1016/j.corsci.2005.05.046.

[52] Y. Tian, Y. Xie, F. Dai, H. Huang, L. Zhong, X. Zhang, Ammonium-grafted graphene oxide for enhanced corrosion resistance of waterborne epoxy coatings, Surf. Coat. Technol. 383 (2020) 125227. https://doi.org/10.1016/j.surfcoat.2019.125227.

[53] S. Wang, Z. Hu, J. Shi, G. Chen, Q. Zhang, Z. Weng, K. Wu, M. Lu, Green synthesis of graphene with the assistance of modified lignin and its application in anticorrosive waterborne epoxy coatings, Appl. Surf. Sci. 484 (2019) 759–770. https://doi.org/10.1016/j.apsusc.2019.03.229.